Cell, Vol. 115, 229–240, October 17, 2003, Copyright ©2003 by Cell Press

The Structure of ClpB: A Molecular Chaperone that Rescues Proteins from an Aggregated State

Sukyeong Lee,[1] Mathew E. Sowa,[1] Yo-hei Watanabe,[2] Paul B. Sigler,[3,4] Wah Chiu,[1] Masasuke Yoshida,[2] and Francis T.F. Tsai[1,*]

[1]Verna and Marrs McLean Department of Biochemistry and Molecular Biology
Baylor College of Medicine
Houston, Texas 77030

[2]Chemical Resources Laboratory
Tokyo Institute of Technology
Yokohama 226-8503
Japan

[3]Department of Molecular Biophysics and Biochemistry
and the Howard Hughes Medical Institute
Yale University
New Haven, Connecticut 06511

Summary

Molecular chaperones assist protein folding by facilitating their "forward" folding and preventing aggregation. However, once aggregates have formed, these chaperones cannot facilitate protein disaggregation. Bacterial ClpB and its eukaryotic homolog Hsp104 are essential proteins of the heat-shock response, which have the remarkable capacity to rescue stress-damaged proteins from an aggregated state. We have determined the structure of *Thermus thermophilus* ClpB (*T*ClpB) using a combination of X-ray crystallography and cryo-electron microscopy (cryo-EM). Our single-particle reconstruction shows that *T*ClpB forms a two-tiered hexameric ring. The ClpB/Hsp104-linker consists of an 85 Å long and mobile coiled coil that is located on the outside of the hexamer. Our mutagenesis and biochemical data show that both the relative position and motion of this coiled coil are critical for chaperone function. Taken together, we propose a mechanism by which an ATP-driven conformational change is coupled to a large coiled-coil motion, which is indispensable for protein disaggregation.

Introduction

Proteins must fold correctly to attain their biological function. Concurrently, protein misfolding and aggregation contribute to many human diseases such as Alzheimer's disease, type II diabetes, and prion-mediated infections. While conventional chaperones assist protein folding by promoting forward folding and preventing aggregation, they cannot facilitate protein disaggregation.

ClpB and Hsp104 (ClpB/Hsp104) are ATP-dependent molecular chaperones, which belong to the Hsp100 family of ATPases associated with diverse cellular activities (AAA^+) (Schirmer et al., 1996; Neuwald et al., 1999; Vale, 2000; Ogura and Wilkinson, 2001). Hsp100 proteins contain either two (class 1) or one (class 2) nucleotide binding domain (NBD) (Schirmer et al., 1996) that features the Walker A and B motifs which are found in many nucleotide binding proteins (Walker et al., 1982). ClpB/Hsp104 is a member of the class 1 family, but is distinct from other Hsp100 proteins because ClpB/Hsp104 contains a longer middle region, known as the "linker" or "spacer," that separates the two NBDs (Schirmer et al., 1996). This linker is essential for chaperone activity (Cashikar et al., 2002), but its precise structure and function have not been determined. Moreover, unlike other Hsp100 proteins, such as ClpA and ClpX, ClpB/Hsp104 does not associate with the structurally and functionally unrelated ClpP protease, and does not direct the degradation of its substrate proteins (Weber-Ban et al., 1999; Wickner et al., 1999; Kim et al., 2000a). Rather, ClpB/Hsp104 has the remarkable capacity to rescue proteins from an aggregated state by mediating the disaggregation of stress-damaged proteins (Parsell et al., 1994b). The full recovery of active proteins requires the assistance of the DnaK/Hsp70 chaperone system (Glover and Lindquist, 1998; Goloubinoff et al., 1999; Mogk et al., 1999; Motohashi et al., 1999; Zolkiewski, 1999). However, the mechanism of this bichaperone network remains elusive.

Currently, little is known about the structure-function relationship of ClpB/Hsp104 molecular chaperones due to the lack of an atomic structure of the functional assembly. This structural information is essential, however, in order to understand the mechanism by which members of the ClpB/Hsp104 family mediate protein disaggregation. It has been suggested that ClpB/Hsp104 forms higher-order oligomers in a nucleotide-, protein concentration-, and salt concentration-dependent manner (Parsell et al., 1994a; Zolkiewski et al., 1999; Kim et al., 2000b; Schlee et al., 2001; Watanabe et al., 2002). The structural organization of the functional assembly, however, is controversial. While it has been proposed that *E. coli* ClpB forms a heptamer (Kim et al., 2000b), it has been suggested that Hsp104 forms a hexameric ring-shaped structure (Parsell et al., 1994a).

Here we present the 3.0 Å resolution crystal structure of full-length *T*ClpB in complex with adenosine 5′-(β,γ-imido)triphosphate (AMPPNP) and the single-particle reconstruction of the *T*ClpB-AMPPNP hexamer at ~21 Å resolution. The most remarkable structural feature is the 85 Å long, leucine-rich coiled coil, which consists of the ClpB/Hsp104-linker and resembles in structure the shape of a two-bladed propeller. The structure of the *T*ClpB hexamer, together with our mutagenesis and sulfhydryl crosslinking data, suggests a mechanism by which ClpB utilizes an ATP-driven conformational change to mediate the disaggregation of high molecular weight aggregates.

Results and Discussion

Structure Determination

*T*ClpB was expressed and purified as described in the Experimental Procedures. A number of different crystal

*Correspondence: ftsai@bcm.tmc.edu

[4]Deceased.

Table 1. Data Collection, MAD Phasing, and Refinement Statistics

	Native 1	Native 2	Se-Met		
Data Collection Statistics					
Space group	$P2_12_12_1$				
Unit cell	a = 107.8 Å, b = 138.4 Å, c = 212.2 Å	a = 109.2 Å, b = 139.6 Å, c = 213.0 Å			
X-ray source	NSLS, X25	NSLS, X25	APS, SBC-19ID		
Wavelength (Å)	λ = 1.072	λ = 1.100	λ_1 = 0.9793	λ_2 = 0.9795	λ_3 = 1.0197
Resolution (Å)	48.0–3.0	48.8–3.2	47.7–3.6	47.7–3.5	47.7–3.5
Completeness (%)[a]	91.4 (37.1)	95.9 (70.4)	98.7 (99.7)	97.0 (82.6)	95.1 (71.0)
R_{sym}[a,b]	0.053 (0.381)	0.036 (0.275)	0.075 (0.420)	0.069 (0.359)	0.057 (0.355)
I/σ[c]	19.1	27.7	13.5	15.1	16.7
MAD Phasing Statistics					
R_{iso}[d]	0.687	0.182	0.042	0.053	
R_{Cullis}[e]			0.677	0.797	
Phasing $Power_{cen/iso}$[f]			1.1	1.0	
Phasing $Power_{acen/iso}$[f]			1.6	1.5	
Phasing $Power_{acen/ano}$[f]			2.4	2.4	0.6
Figure of Merit[g]		0.37 (centric)	0.54 (acentric)		
Refinement Statistics					
Resolution (Å)	48.0–3.0	48.8–3.2			
R_{cryst}/R_{free}	0.263/0.307	0.265/0.308			
rmsd bond length	0.005 Å	0.008 Å			
rmsd angles	1.13°	1.38°			

[a] Values for the highest resolution shell are given in parentheses.
[b] $R_{sym} = \Sigma_{hkl} |I(hkl) - \langle I(hkl)\rangle| / \Sigma_{hkl} I(hkl)$, where $\langle I(hkl)\rangle$ is the mean of the symmetry equivalent reflections of I(hkl).
[c] Based on unmerged data.
[d] $R_{iso} = \Sigma|F_{PH} - F_P|/\Sigma F_P$, where F_P is the low energy remote (λ_3), and F_{PH} are the peak (λ_1), inflection (λ_2), and native structure factor amplitudes, respectively.
[e] $R_{Cullis} = \Sigma||F_{PH} \pm F_P| - F_H^{calc}|/\Sigma|F_{PH} \pm F_P|$ for centric reflections only.
[f] Isomorphous phasing power $= \Sigma|F_H|/\Sigma||F_{PH}^{obs}| - |F_{PH}^{calc}||$; anomalous phasing power $= \Sigma|F''_H|/\Sigma||AD_{obs}| - |AD_{calc}||$.
[g] Figure of Merit = weighted mean of the cosine of the deviation from α_{best}.

forms were obtained under a variety of conditions, which diffracted poorly (data not shown). After extensive screening of potential crystallization conditions, we obtained a crystal form of *T*ClpB in the presence of AMPPNP, which diffracted to moderate resolution using synchrotron radiation.

The crystal structure of the *T*ClpB-AMPPNP complex was solved by the multiple wavelength anomalous dispersion (MAD) technique, followed by model refinement with diffraction data extending to 3.0 Å resolution. Table 1 summarizes the data collection, phasing, and refinement statistics. There are three independent representations of full-length *T*ClpB in the crystallographic asymmetric unit with each *T*ClpB monomer containing two bound AMPPNP molecules. The current structure includes residues 4–234, 246–271, 291–636, and 651–850 (Figure 1).

Structure of the *T*ClpB Monomer

The *T*ClpB monomer can be divided into five distinct domains: the N-terminal domain (residues 4–135); the D1-large domain or NBD1 (residues 151–331); the D1-small domain (residues 332–535) that contains the ClpB/Hsp104-linker; the D2-large domain or NBD2 (residues 545–756); and the D2-small domain (residues 757–850) (Figure 2A). The N-terminal domain of *T*ClpB is mostly α-helical with two short parallel β strands inserted near its N terminus (Figure 2A). While the overall structure of this domain is similar to that of the isolated N-terminal domain of *E. coli* ClpB (Li and Sha, 2003), it does not contain a pseudo 2-fold symmetry.

The N-terminal domain is connected to NBD1 through a flexible linker (residues 136–150) (Figure 2A). The structure of NBD1 has a RecA-like mononucleotide binding fold but with an additional antiparallel β strand inserted at the beginning of the RecA-like domain (Figure 2A). The NBD1 of full-length *T*ClpB and the isolated NBD1 of *E. coli* ClpB (Li and Sha, 2002) show a root mean squared deviation (rmsd) of only 0.86 $\pm$ 0.03 Å when superimposed pairwise through 141 out of 181 Cα atoms. The structure of the isolated *E. coli* NBD1, however, did not contain a bound nucleotide, probably as the result of an incomplete nucleotide binding cleft. In our structure, AMPPNP is bound in an *anti* conformation and is buttressed by the Walker A motif (P-loop), the loop connecting helices B2 and B3 in NBD1, and the conserved I340, L344, and I382 of the D1-small domain (Figure 2C). The 6-amino group of the adenine base donates a hydrogen bond to the carbonyl oxygen of the I173 main chain (Figure 2C). Nucleotide binding, however, would also be compatible with a hydrogen bond acceptor of the 6-keto group of guanine nucleotides.

The D1-small domain consists of a bundle of four α helices with two short parallel β strands and a long coiled coil, the ClpB/Hsp104-linker, which is inserted between helix C3 and β strand c2 (Figure 2B). This long

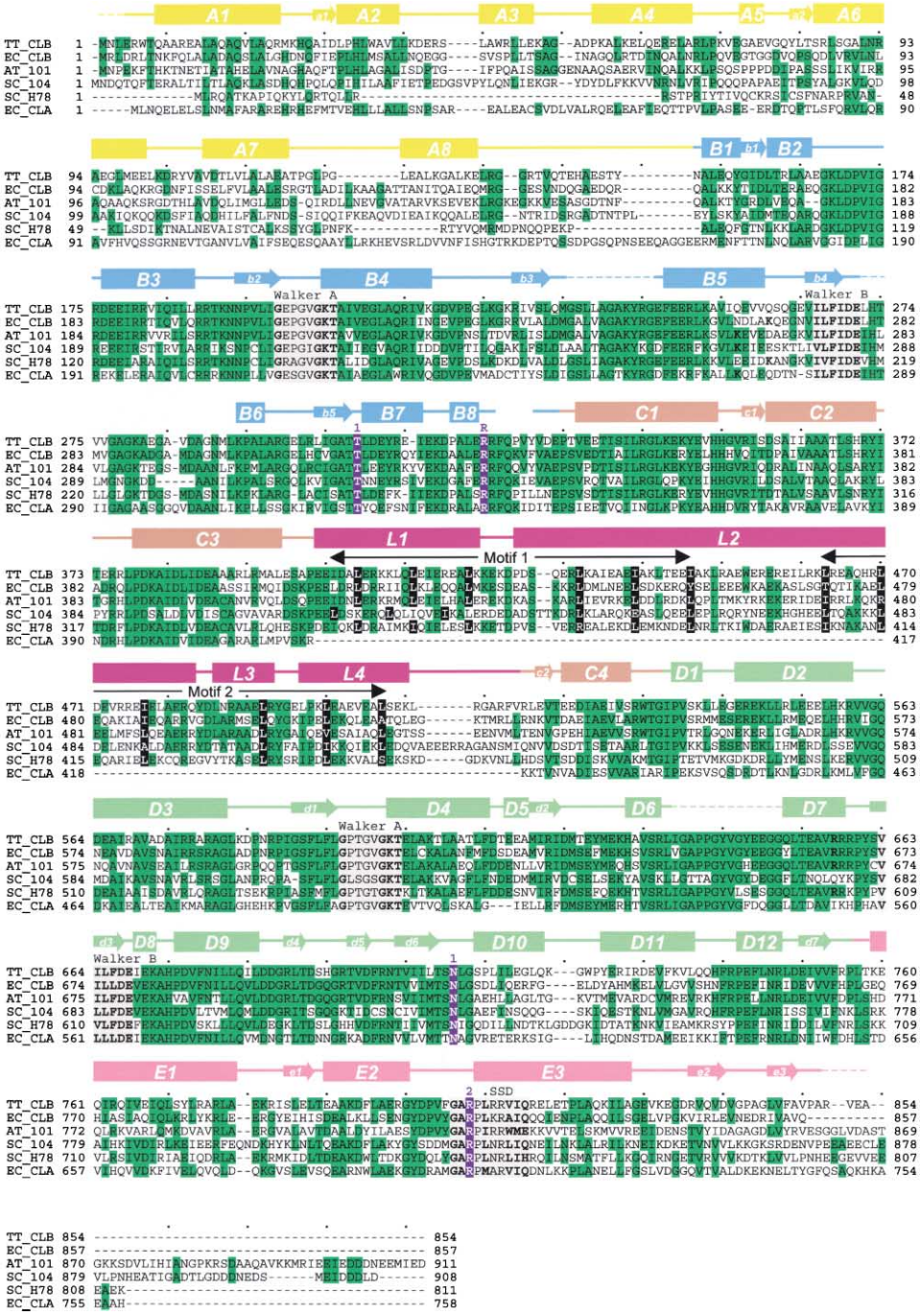

Figure 1. Sequence Alignment and Secondary Structure Elements of ClpB/Hsp104

TT_CLB: *T. thermophilus* ClpB; EC_CLB: *E. coli* ClpB; AT_101: *A. thaliana* Hsp101; SC_104: *S. cerevisiae* Hsp104; SC_H78: *S. cerevisiae* Hsp78; and EC_CLA: *E. coli* ClpA. A black dot above the sequence marks every ten amino acids. Secondary structure elements are shown as bars (α helices) and arrows (β strands), and are labeled in upper case (α helices) and lower case (β strands) letters. The N-terminal domain (A) is colored in gold; the D1-large domain or NBD1 (B) in cyan; the D1-small domain (C) in salmon; the ClpB/Hsp104-linker (L) in purple; the D2-large domain or NBD2 (D) in green; and the D2-small domain (E) in pink. These nomenclature and color designations are used throughout in all figures. Dotted lines represent the points at which the electron density for *T*ClpB is not interpretable. Residues that are part of the Walker A, Walker B, and SSD motifs are boxed in gray with the signature residues shown in bold. Sensor 1 (1), sensor 2 (2), and the arginine-finger (R) are shown in bold surrounded by a blue box. The black arrows indicate the sequence of the leucine zipper-like motifs. Residues that are part of the heptad repeats are shown in bold surrounded by a black box.

coiled coil is composed of two shorter coiled-coil motifs, consisting of helices L1 and L2 (motif 1), and L2 and L3/L4 (motif 2), respectively, and share a common α-helix (L2), 85 Å in length (Figure 2B). Each of the two shorter motifs is reminiscent to that of leucine zippers typically found in eukaryotic transcription factors

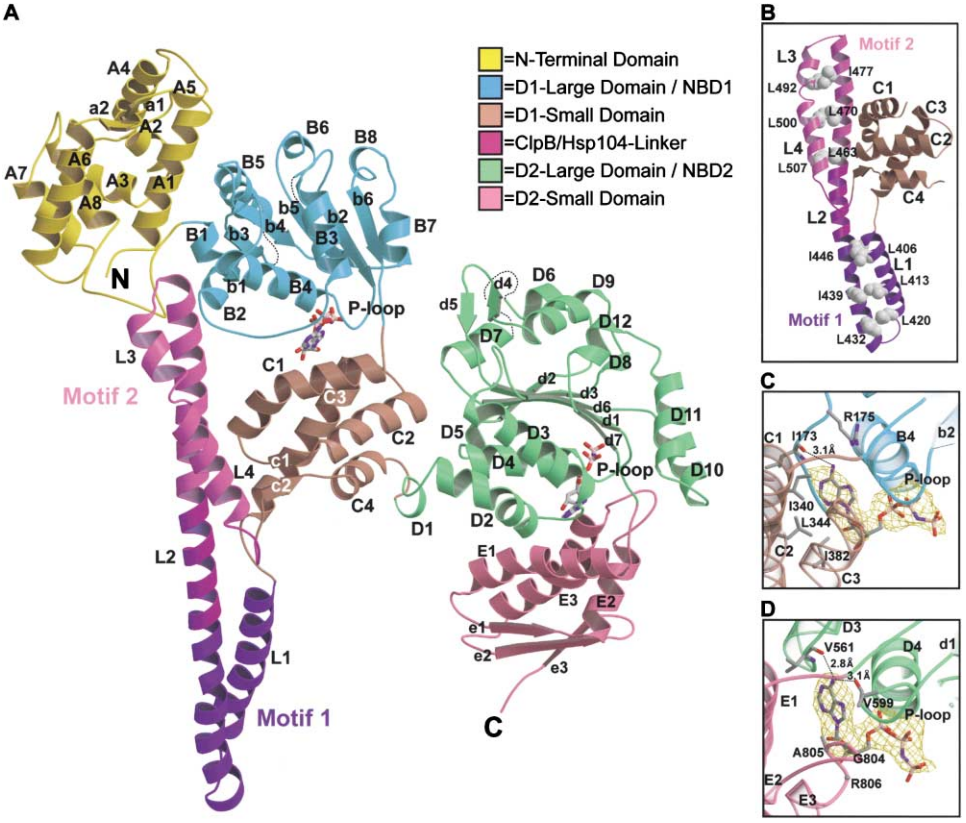

Figure 2. Structure of the *T*ClpB Monomer

(A) Ribbon drawing of one *T*ClpB monomer. Motif 1 and motif 2 of the ClpB/Hsp104-linker are shown in different hues. All secondary structure elements are labeled and the locations of the P-loops are shown. AMPPNP is depicted as a stick model.

(B) The long coiled coil resembles in structure the shape of a two-bladed propeller and consists of two smaller coiled-coil motifs (motif 1 and motif 2) shown in different hues. Residues that are part of the leucine-rich heptad repeat are shown as CPK models.

(C) Structure of the nucleotide binding cleft of the D1 domain. The simulated annealed omit map was calculated using phases derived from the final model with AMPPNP omitted and is contoured at 3.5 σ. AMPPNP is shown as stick model. Hydrogen bonds are indicated by dotted lines.

(D) Structure of the nucleotide binding cleft of the D2 domain. The simulated annealed omit map was calculated as described in (C). AMPPNP is shown as stick model. Hydrogen bonds are indicated by dotted lines. Figures were prepared with the programs MOLSCRIPT (Kraulis, 1991), BOBSCRIPT (Esnouf, 1997), and RASTER3D (Merritt and Bacon, 1997).

(O'Shea et al., 1991; Ellenberger et al., 1992). Unlike the classical leucine zipper motif, however, motif 1 and motif 2 consist of two antiparallel α helices with only three consecutive leucine-rich heptad repeats (Figure 2B).

The D1-small domain is connected to NBD2 via helix D1 (Figure 2A), which may function as a hinge allowing motion between the D1 domain (residues 151–535) and the D2 domain (residues 545–850). The structure of NBD2 also has a RecA-like fold with a β-hairpin motif inserted after helix D9 (Figure 2A). Similar to NBD1, AMPPNP is bound in an *anti* conformation (Figure 2D). The nucleotide is buttressed by the P-loop, the loop connecting helices D2 and D3 in NBD2, helix E1, and the conserved G804, A805, and R806 (sensor 2) of the "sensor- and substrate-discrimination" (SSD) motif (Smith et al., 1999) (Figure 2D). It should be noted, however, that the long and flexible side chain of R806 is disordered in all three representations of *T*ClpB. Specificity for adenine nucleotides is provided through base-specific interactions. The 6-amino group of the adenine base forms a bifurcated hydrogen bond with the main chain carbonyl oxygen of V561 and V599, respectively (Figure 2D). In contrast to NBD1, this interaction would be incompatible with a hydrogen bond acceptor of the 6-keto group of guanine nucleotides.

The D2-small domain has a mixed α/β structure and a similar topology as the D1-small domain (Figure 2A). However, the D2-small domain lacks the long coiled-coil insertion, and instead of helix C4, contains a β strand (e3) that is part of a three stranded β-pleated sheet.

The overall topology of the *T*ClpB monomer is similar to that of *E. coli* ClpA whose structure has been reported recently (Guo et al., 2002). However, the relative orientation and position of the D1 domain differ approximately by a 50° rotation and a 24 Å translation when the crystal structures of ClpA and *T*ClpB are superimposed pairwise through the Cα atoms of the D2 domain (data not shown). It is possible that ClpA and *T*ClpB adopt different conformations due to the different crystal lattices or perhaps because ClpA lacks the ClpB/Hsp104-linker that is critical for ClpB function.

Molecular Assembly and Plasticity of *T*ClpB in the Crystal Structure

As noted above, there are three independent representations of full-length *T*ClpB in the crystallographic asym-

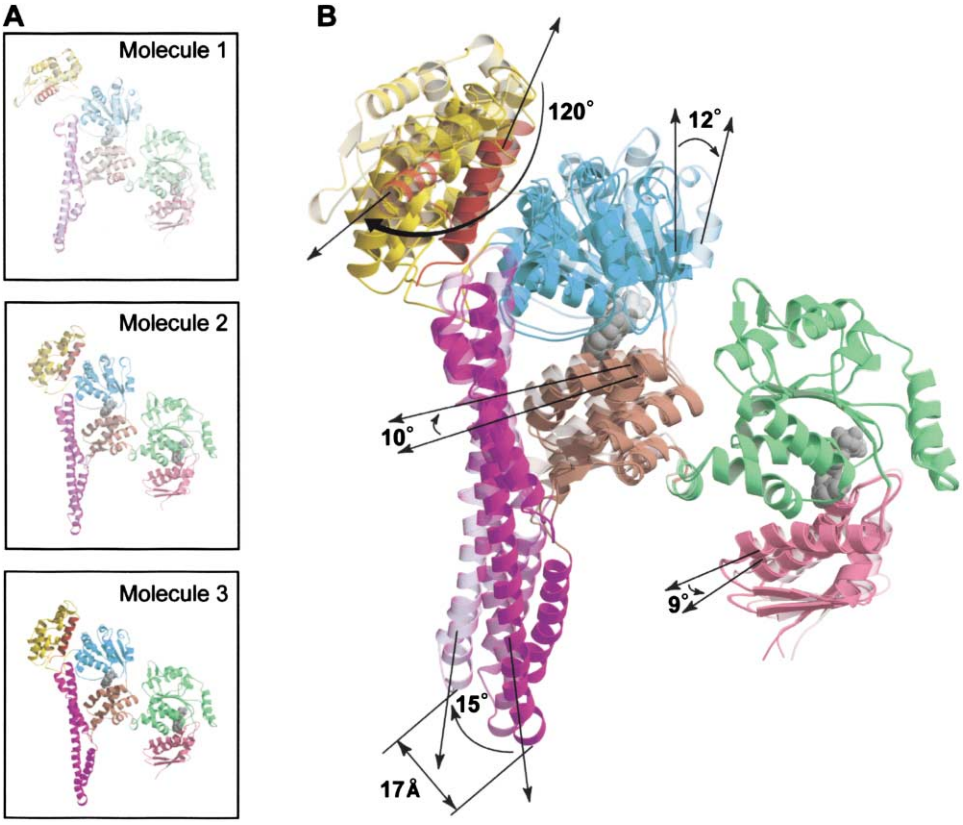

Figure 3. Plasticity of *T*ClpB

(A) Ribbon drawing of the three representations of *T*ClpB colored in different hues. The figure shows that each *T*ClpB molecule adopts a different conformation, even though they are in the same nucleotide bound state. AMPPNP molecules are shown as CPK models and are colored in gray.

(B) The superposition reveals that *T*ClpB is a dynamic molecule. All five domains are mobile as demonstrated by the backbone variations and the large en bloc conformational rearrangement of the N-terminal domains. Since the three *T*ClpB molecules were superimposed through the Cα atoms of NBD2, the latter appears to be static. The arrows indicate the motions of the individual domains. Helix A1 of the N-terminal domain is colored in red for clarity. AMPPNP molecules are shown as in (A).

metric unit (Figure 3A). The three molecules are related approximately by a 60° rotation and a $^1/_6$ translation along the crystallographic 2-fold screw axis parallel to *a*. This arrangement of molecules gives rise to a helical assembly, which extends throughout the crystal and forms a hexameric ring structure when viewed in projection (data not shown). It is important to note that, in the crystal, each of the three *T*ClpB molecules in the asymmetric unit adopts a different conformation, even though they are in the same nucleotide bound state (Figure 3A). This suggests that *T*ClpB is a dynamic molecule that can undergo large conformational rearrangements. The superposition of the three *T*ClpB molecules highlights the remarkable plasticity of *T*ClpB (Figure 3B). Each *T*ClpB molecule is conformationally different as demonstrated by the backbone variations and the large en bloc rearrangement of the N-terminal domain. When the three molecules are superimposed pairwise through the Cα atoms of NBD2 (rmsd of 0.23 ± 0.02 Å), the orientation of the N-terminal domain of molecule 1 is rotated by 120° and 117° relative to that of molecules 2 and 3, respectively (Figure 3B). This demonstrates that the N-terminal domain is mobile and does not form a tight interface with NBD1.

The superposition also reveals that the long coiled coil is mobile (Figure 3B). The position of the tip of motif 1 swings by up to 17.3 Å when the three molecules are superimposed through the Cα atoms of NBD2 (Figure 3B) and up to 9.6 Å when superimposed through NBD1 (data not shown). The structure of the ClpB/Hsp104-linker suggests that the conformation and perhaps the motion of the coiled coil are important for protein disaggregation.

Structure of the *T*ClpB Hexamer

To determine the oligomeric state of the functional *T*ClpB assembly, we have examined the structure of the *T*ClpB-AMPPNP complex using cryo-EM. The initial model was generated from reference-free classification of individual *T*ClpB particles, without applying any symmetry, using the EMAN software package (Ludtke et al., 1999). Projection views of the single-particle reconstruction with C_6 symmetry applied during refinement most closely matched their corresponding class averages, indicating that *T*ClpB forms a hexamer (Figure 4A).

Our reconstruction shows that the *T*ClpB hexamer forms a two-tiered ring structure with a height of 90 Å, a diameter of 140 Å for the bottom ring, and a diameter of 150 Å for the top ring (Figure 4A). There is an ~16 Å wide hole in the top ring and six smaller openings on

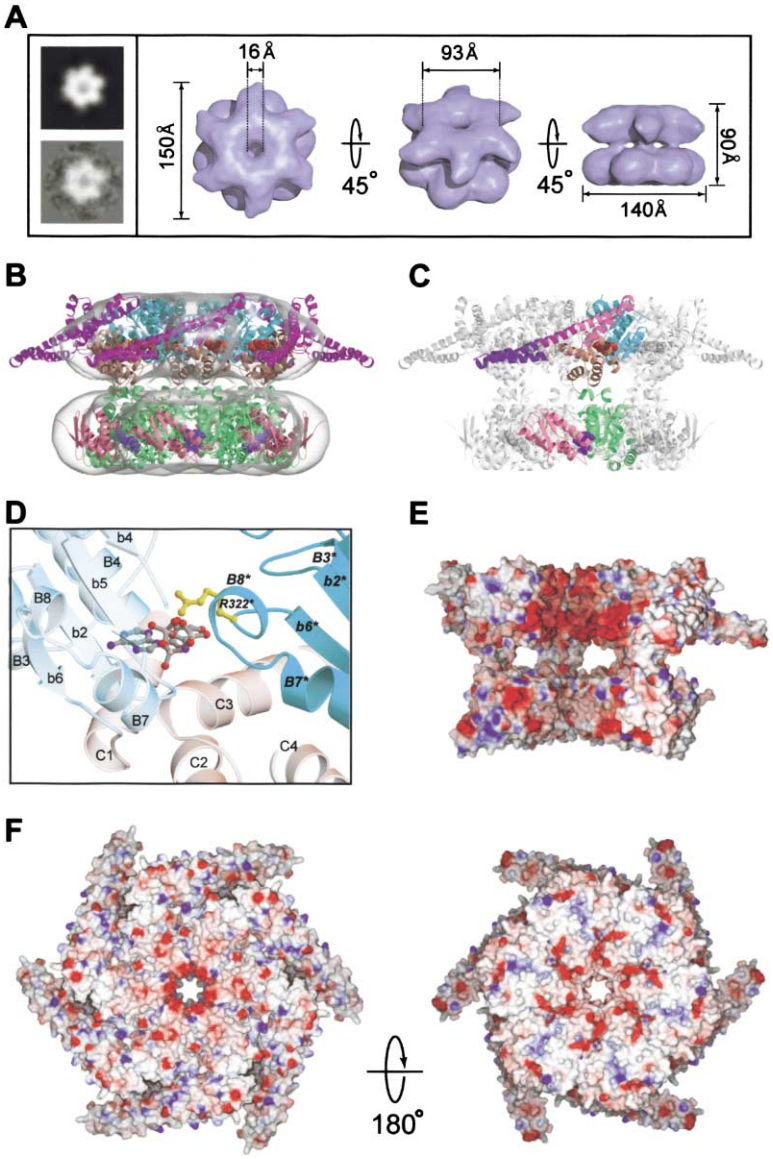

Figure 4. Structure of the *T*ClpB Hexamer

(A) Single-particle reconstruction of the *T*ClpB-AMPPNP hexamer. (Left) The top image shows a projection of the *T*ClpB reconstruction and the bottom image shows the corresponding class average. Only the top image has C_6 symmetry applied. The box is 244 Å across. (Right) The reconstruction has a height of 90 Å, and a diameter of 150 Å (top ring) and 140 Å (bottom ring), respectively. There is a central hole in the top ring (~16 Å) and six smaller openings on the lateral surface of the molecule.

(B) The reconstruction is shown as a semi-transparent surface, with the structure of the N-terminal domain deleted *T*ClpB-AMPPNP hexamer docked in, demonstrating the goodness of fit. The N-terminal domain and part of the ClpB/Hsp104-linker are not visible in our reconstruction since they are mobile. AMPPNP molecules are shown as CPK models and are colored in red (NBD1) and blue (NBD2).

(C) The quaternary structure of the *T*ClpB-AMPPNP hexamer shows that the NBD1 and NBD2 of the same *T*ClpB subunit are positioned directly above each other with the long coiled coil located on the outside of the hexamer. For clarity, only one *T*ClpB subunit is colored. AMPPNP molecules are shown as in (B).

(D) Molecular interface between the NBD1s of adjacent subunits. The figure shows a close-up view of the arginine finger (yellow), which reaches across the subunit interface to facilitate nucleotide hydrolysis in the neighboring subunit. AMPPNP is shown as ball-and-stick model. The asterisk indicates a structure element from the adjacent subunit contributing the arginine finger.

(E) Electrostatic surface potential along the pore (side view). Two *T*ClpB monomers have been removed from the hexamer to illustrate the electrostatic potential of the inner surface. Blue and red represent regions of positive and negative potential at the 23 k_BT/e level as calculated using DelPhi (Gilson et al., 1987).

(F) Electrostatic surface potential representation of the *T*ClpB hexamer (top and bottom view).

the lateral surface of the molecule (Figure 4A). This quaternary structure gives rise to an internal cavity of ~60,000 Å^3, which is less than half of that reported for ClpA (~140,000 Å^3) (Beuron et al., 1998). The location of the D1 domain was assigned to the top ring based on the protrusion in the *T*ClpB reconstruction, which accounts for part of the ClpB/Hsp104-linker. The N-terminal domain and most of the long coiled coil, however, are not visible in our reconstruction (Figure 4A) and are presumably flexible. This is consistent with our crystal structure, which shows that both of these domains are mobile. Thus, the threshold of the surface rendering was chosen such that the corresponding volume matches the 480 kDa molecular mass of an N-terminal domain truncated *T*ClpB hexamer.

To examine the molecular interactions in the *T*ClpB hexamer, we have fitted the atomic structure of an N-terminal domain truncated *T*ClpB-AMPPNP monomer (molecule 3) into the cryo-EM map (Figure 4B; see Experimental Procedures). Briefly, the D1 and D2 domains of molecule 3 were fitted independently from each other. Residues 536–544, which connect the two fragments, were moved as a rigid body to connect the D1 and D2 domains and to fit the cryo-EM map. The hexamer was generated from the fitted *T*ClpB monomer by applying a 6-fold rotational symmetry matrix. The secondary structure elements of the generated hexamer are all contained within the cryo-EM map, with the exception of the long coiled coil and part of helix D2 (Figure 4B).

In our hexamer, NBD1 is positioned directly above NBD2 of the same subunit (Figure 4C). This quaternary arrangement is different from that proposed for *E. coli* ClpA (Guo et al., 2002). The adenine nucleotide is bound at the interface between two adjacent *T*ClpB subunits.

In the hexamer, R322 contacts the γ-phosphate of AMPPNP from a neighboring molecule (Figure 4D). This is reminiscent of the catalytic arginine, the so-called arginine finger, first reported in the crystal structure of the Ras-GDP-AlF_3/RasGAP complex (Scheffzek et al., 1997). This interaction may not only stabilize the *T*ClpB hexamer, but could also provide the structural basis for cooperativity by "sensing" the functional state of the bound nucleotide in the adjacent subunit and assisting ATP hydrolysis.

While NBD1 and NBD2 line the inside of the top and bottom ring, respectively, the D1-small and D2-small domains are located on the outside of the hexamer, with the long coiled coil being exposed on the surface of *T*ClpB. The calculated electrostatic surface potential map shows that the inside of each ring is mostly acidic (Figure 4E), whereas the outside surface of *T*ClpB is both hydrophobic and polar (Figure 4F). It has been suggested that the D2-small domain is essential for oligomerization since ClpB mutants, which lack this domain, can no longer self-assemble (Barnett et al., 2000; Mogk et al., 2003). Consistent with this finding, in our hexamer the D2-small domain forms a tight interface with the NBD2 of a neighboring subunit (Figure 4C). This interaction could provide the necessary binding energy that stabilizes the functional assembly.

Our model of the *T*ClpB-AMPPNP hexamer reveals that both NBDs contribute toward oligomerization (Figures 4B and 4C). The interface between the D2 domain of adjacent molecules buries ~4800 $Å^2$ of exposed surface area. This area is about 1000 $Å^2$ larger than that for the D1 domain (~3800 $Å^2$). The larger occluded accessible surface area suggests that the D2 domain is responsible for oligomerization, whereas the D1 domain stabilizes the hexamer perhaps in an ATP-dependent manner as suggested by biochemical studies (Kim et al., 2000b; Watanabe et al., 2002).

Structure and Function of the ClpB/Hsp104-Linker

The ClpB/Hsp104-linker has previously been shown to play a crucial role in the interdomain communication between NBD1 and NBD2 (Cashikar et al., 2002). Our structure of *T*ClpB reveals that the long coiled coil is mobile, suggesting that the ClpB/Hsp104-linker may also play an active role in protein disaggregation. To investigate the functional importance of this coiled-coil motion, we generated four sets of mutants by replacing G167/R475, V350/Q467, G353/R464, and R355/E520 with cysteines (Figure 5A). These double mutants were designed based on our crystal structure to form a disulfide bridge under nonreducing but not under reducing conditions. This was possible because there are no cysteine residues in wild-type *T*ClpB.

In the absence of the reducing agent dithiothreitol (DTT), the chaperone activity was impaired in all four mutants (Figure 5B), presumably by restricting the coiled-coil motion through disulfide bond formation. While the chaperone activity of the R355C/E520C mutant was reduced less than half, the G167C/R475C, V350C/Q467C, and G353C/R464C mutants showed a 5-fold to 7-fold decrease in their capacity to rescue heat-aggregated glucose-6-phosphate dehydrogenase (G6PDH) (Figure 5B). Hexamer formation, the ability to hydrolyze ATP, and the casein-induced stimulation of these ATPase activities, however, were maintained as determined by size-exclusion chromatography and by measuring the ATPase activities of wild-type and mutant *T*ClpB (data not shown). In the presence of DTT, the chaperone activity of all four mutant proteins was restored (Figure 5B).

In the G167C/R475C, V350C/Q467C, and G353C/R464C mutants, the coiled coil was immobilized by tethering motif 2 to either NBD1 (G167C/R475C) or the D1-small domain (V350C/Q467C; G353C/R464C) of the same *T*ClpB monomer (Figure 5A). Intermolecular disulfide bond formation was not detected (data not shown). In the R355C/E520C mutant, the coiled coil was immobilized only indirectly by introducing a disulfide bridge between the two β strands of the D1-small domain (Figure 5A). Presumably, the latter allows some coiled-coil motion, which could explain the higher chaperone activity with respect to the other mutants (Figure 5B). Our sulfhydryl crosslinking results demonstrate that the capacity of *T*ClpB to rescue proteins from an aggregated state correlates with the degree of motion of the long coiled coil.

To investigate whether the relative position of the coiled coil is essential for protein disaggregation, we replaced L396, L460, or L396/L460 with alanines (Figure 5A). These leucine residues are located at the interface between the ClpB/Hsp104-linker and the D1-small domain (Figures 5A and 5C), and stabilize the position of the long coiled coil. While the chaperone activity of the L460A mutant was reduced 4-fold, the L396A mutant showed a 9-fold decrease and the L396A/L460A double mutant a more than 20-fold decrease in their capacity to rescue heat-aggregated G6PDH (Figure 5B). The ATPase activities, casein-induced stimulation, and the ability to self-assemble, however, were unaffected, demonstrating that these mutants were functional in other respects (data not shown). It is possible that the leucine to alanine mutations may have interfered with substrate binding to *T*ClpB, even though L396 and L460 are buried (Figure 5C). It is more likely, however, that our mutations have disrupted the correct positioning and perhaps the motion of the long coiled coil, which in turn abolished the ability of *T*ClpB to disaggregate proteins. Taken together, our results demonstrate that the protein disaggregation and ATPase activities of *T*ClpB can be uncoupled and, more importantly, support the notion that the relative position and motion of the long coiled coil are critical for chaperone activity.

Mechanistic Model for Protein Disaggregation by ClpB

A number of different mechanisms have been proposed by which members of the AAA^+ family modulate the conformational state of their substrate proteins (Vale, 2000; Ogura and Wilkinson, 2001). It has been suggested that a hexameric ring structure may provide a framework for binding target proteins at multiple sites and that ATP-driven conformational changes could provide the necessary mechanical force to modulate substrate proteins (Vale, 2000).

Our results show that both the relative position and motion of the long coiled coil are essential for *T*ClpB's

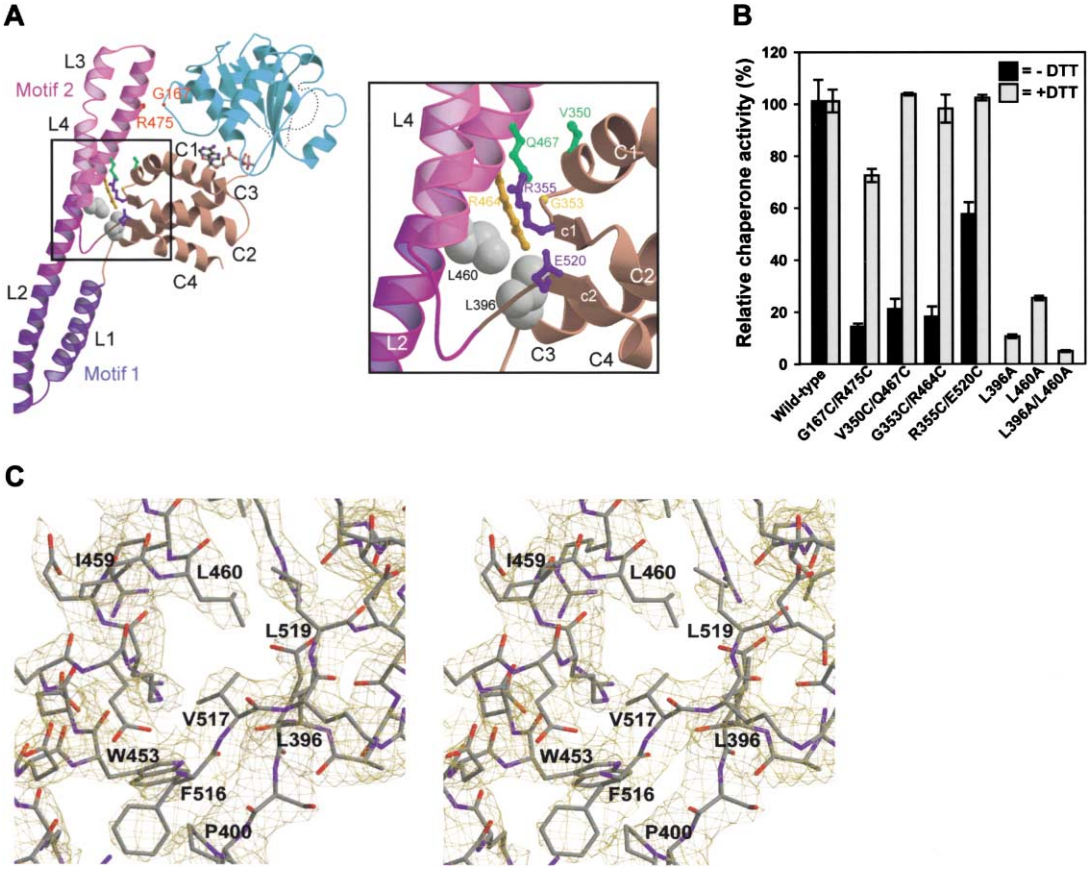

Figure 5. Structure and Function of the ClpB/Hsp104-Linker

(A) Ribbon drawing of the D1 domain. Motif 1 and motif 2 of the ClpB/Hsp104-linker are shown in different hues. Residues that were mutated G167/R475 (red), V350/Q467 (green), G353/R464 (yellow), and R355/E520 (blue) are depicted as ball-and-stick, and L396 and L460 as space-filling CPK models.

(B) Chaperone activity assay. The assays were carried out either in the absence (black bars) or in the presence of 5 mM DTT (gray bars). The chaperone activities of the leucine to alanine mutations were only measured in the presence of DTT. The values shown are the average chaperone activities of each mutant relative to that of wild-type and were derived from at least three independent measurements.

(C) Stereo drawing of the interface between the ClpB/Hsp104-linker and the D1-small domain. The composite annealed omit map was calculated using phases derived from the final model and is contoured at 1.0 σ.

ability to rescue proteins from an aggregated state. We have further demonstrated that the chaperone activity correlates with the degree of motion of the long coiled coil. While the nature and direction of this motion are unknown, the long coiled coils presumably move in concert in order to avoid steric interference with the long coiled coil of a neighboring subunit. A concerted coiled-coil motion that causes motif 1 and motif 2 of adjacent subunits to move in opposite directions could generate the required mechanical force to pull apart large aggregates. Interestingly, ClpA in complex with ClpP has also been shown to disaggregate proteins in vitro, but unlike the ClpB-DnaK bichaperone system, is unable to do so in vivo (Dougan et al., 2002), presumably due to the lack of the long coiled coil. This indicates that ClpB/Hsp104 is the principal protein disaggregation machine inside the cell and suggests that ClpB/Hsp104 has an additional disaggregation activity not found in other Hsp100 proteins.

We propose that ClpB has at least two functions: to disaggregate high molecular weight aggregates into smaller aggregates and to assist in the resolubilization of medium-size aggregates together with the DnaK chaperone system (Figure 6). We propose that the ClpB hexamer first recognizes and binds large aggregates between motif 1 and motif 2 of adjacent ClpB subunits. It is conceivable that ClpB only recognizes aggregates that are large enough to bind simultaneously to motif 1 and motif 2. This is consistent with the observation that ClpB is required for the efficient solubilization of high molecular weight aggregates, but is dispensable for the disaggregation of small aggregates (Diamant et al., 2000). We favor a mechanism by which a small ATP-driven conformational change within the D1 domain is coupled to a large coiled-coil motion, which could provide the necessary leverage to dissociate large aggregates (Figure 6). This may be achieved by an opening or closing of the nucleotide binding cleft or a small rotation of the D1-small domain relative to the D1-large domain as observed in the crystal structures of the different nucleotide bound states of HslU, a member of the class 2 family of Hsp100 proteins (Wang et al., 2001). While

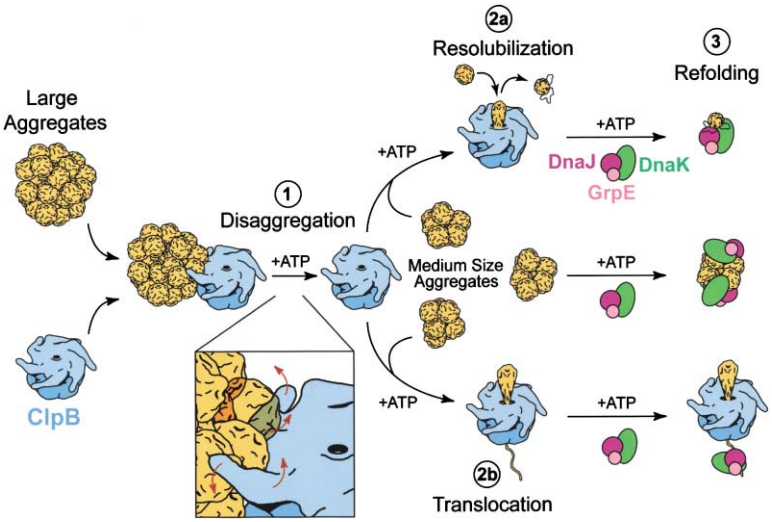

Figure 6. Mechanistic Model for Protein Disaggregation by ClpB

(1) Disaggregation of high molecular weight aggregates, which bind to the outside of the ClpB hexamer. We propose that ClpB recognizes only large aggregates that can bind simultaneously to motif 1 and motif 2 of neighboring ClpB subunits. The red arrows indicate the concerted and opposite motion of motif 1 and motif 2 in adjacent subunits, which could generate the mechanical force to pull apart large aggregates. (2) Resolubilization of medium size aggregates or misfolded polypeptides. Following protein disaggregation, the smaller aggregates are either recognized by the DnaK chaperone system directly or enter the cavity of the ClpB hexamer, where they are resolubilized perhaps by (2a) a "capture-and-release" or (2b) a translocation mechanism. (3) Refolding of small aggregates or polypeptides by the DnaK chaperone system.

it is currently unknown how ClpB/Hsp104 binds its substrates and what structures it may recognize, it is possible that the binding of aggregated proteins is further stabilized through interactions with other regions in ClpB/Hsp104, such as the N-terminal and D2-small domains, which could provide additional anchoring points. However, the N-terminal domain has been shown to be dispensable for chaperone activity (Clarke and Eriksson, 2000; Beinker et al., 2002; Mogk et al., 2003) and it is unlikely that a conformational change in this domain alone would be sufficient to generate the required mechanical force to facilitate protein disaggregation.

The disaggregation of high molecular weight aggregates by ClpB would create smaller, medium-size aggregates that could expose hydrophobic surfaces, which are recognized in turn by the DnaK chaperone system (Goloubinoff et al., 1999). It is conceivable, however, that the ClpB hexamer may also assist in the resolubilization of these medium-size aggregates perhaps through a "capture-and-release" or translocation mechanism (Figure 6), in a similar manner as shown for other Hsp100 proteins (Ortega et al., 2000; Ishikawa et al., 2001). This would be consistent with multiple substrate binding sites in ClpB/Hsp104 as proposed by others (Park et al., 1993; Smith et al., 1999; Barnett et al., 2000; Cashikar et al., 2002; Tek and Zolkiewski, 2002). While the geometry and the extent of resolubilization remain unclear, it is conceivable that the DnaK chaperone system could bind to the polypeptides immediately upon release from the ClpB hexamer, thereby stabilizing the folding intermediates and preventing reaggregation (Figure 6).

Conclusion

Our results demonstrate that *T*ClpB is a hexamer and that both NBDs contribute toward self-assembly in the AMPPNP-bound state. The ClpB/Hsp104-linker forms a long and mobile coiled coil that is located on the outside of the hexamer. We have further shown through structure-based targeted mutagenesis that the relative position and motion of this coiled coil is critical for chaperone activity and that the capacity of ClpB to rescue proteins from an aggregated state correlates with the degree of coiled-coil motion. The conformational changes that occur in the *T*ClpB hexamer during the ATPase cycle, however, are currently unknown and require further structural studies of the functional assembly in different nucleotide bound states.

Experimental Procedures

Protein Preparation

*T*ClpB was expressed and purified essentially as described (Motohashi et al., 1999). Briefly, *E. coli* BL21 (DE3) cells were transformed with an expression plasmid harboring the *clpB* gene under the control of the T7 RNA polymerase promoter (Motohashi et al., 1999). Cells were grown at 37°C to mid-log phase in Luria-Bertani medium and induced by the addition of 1 mM IPTG. The cells were grown for a further 3 hr after induction and harvested at 4°C. The *T*ClpB hexamer was purified by several column chromatography steps in the following order: DEAE-Sepharose, Butyl-Sepharose, Mono-Q, and Superose 6. For the MAD analysis, seleno-methionyl *T*ClpB was prepared by transforming an *E. coli* methionine auxotroph strain, B834 (DE3) pLysS. Cells were grown in defined medium supplemented with 50 mg/L seleno-DL-methionine (Sigma-Aldrich). Preparation of seleno-methionyl *T*ClpB was otherwise identical to wild-type protein.

Crystallization and Data Collection

Crystals were grown by the hanging drop vapor-diffusion method by mixing an equal volume of protein sample (15 mg/ml) in 10 mM Tris-HCl [pH 7.6], 100 mM NaCl, 10 mM $MgCl_2$, 5% glycerol, and 5 mM AMPPNP (Sigma-Aldrich) with reservoir solution consisting of 4% (w/v) polyethylene glycol 4000, 200 mM sodium acetate pH 4.1, 200 mM KCl, and 20% glycerol. Data were collected at NSLS X25 (native) and APS SBC-ID19 (MAD), and were processed using the HKL2000 software package (Otwinowski and Minor, 1997).

Crystal Structure Determination and Refinement

The structure of *T*ClpB was solved initially at 3.6 Å resolution using the MAD technique. Selenium sites were identified from the difference in intensity between the Bijvoet pairs of the peak anomalous wavelength data. Heavy atom parameters were refined with the program SHARP (de la Fortelle and Bricogne, 1997). The resulting phases were used to calculate the electron density map, which was only partially interpretable and could not be further improved by noncrystallographic symmetry (NCS) averaging. A polyalanine model was built into this map using the program O (Jones et al., 1991). The resulting model was used to calculate a new set of NCS operators: four NCS operators for each of the three representations

of *T*ClpB in the asymmetric unit. Multidomain averaging using DMMULTI (CCP4, 1994) improved the 3.6 Å resolution experimental electron density map, which allowed the tracing of all three *T*ClpB molecules. Cycles of rebuilding and refinement were carried out using the programs O (Jones et al., 1991) and CNS (Brünger et al., 1998), respectively, while the data were extended to 3.2 Å resolution (native 2). During the course of refinement, the NCS constraints were released as validated by monitoring the R_{free}. However, in the 3.2 Å resolution crystal structure, no density for the γ-phosphate of AMPPNP was observed (data not shown). Crystals were not obtained, however, when AMPPNP was replaced with ADP. It appears that AMPPNP was hydrolyzed during crystal formation perhaps as a result of the acidic nature of our crystallization condition. The 3.0 Å resolution structure of the *T*ClpB-AMPPNP complex (native 1) was determined subsequently by difference Fourier in combination with multidomain rigid body refinement techniques. The backbone geometry of the refined model has 82.5% of the residues in the most favored conformations and no residues in disallowed regions of the Ramachandran plot.

Cryo-EM

The *T*ClpB hexamer was isolated by size-exclusion chromatography and incubated with AMPPNP at 55°C to generate the *T*ClpB-AMPPNP complex. Following complex formation, the *T*ClpB-AMPPNP hexamer was crosslinked with 0.01% glutaraldehyde as described (Watanabe et al., 2002) to stabilize the hexameric assembly. Four μl of the crosslinked sample were applied to glow discharged copper grids and frozen in liquid ethane. *T*ClpB was examined at −180°C using a JEOL JEM-2010F electron microscope operated at 200 keV. Low dose images ($\sim$15–18 $e^-/Å^2$) were recorded on Kodak SO-163 film at a nominal magnification of 50,000×. Electron micrographs of ice-embedded *T*ClpB were digitized using a Nikon Super CoolScan 8000 at a step size of 6.35 μm and were then computationally filtered to a final resolution of 2.54 Å/pixel for image processing. Individual *T*ClpB particles are clearly observed under these conditions (data not shown).

Image Processing and Refinement

All image processing was done using the EMAN single particle reconstruction suite of programs (Ludtke et al., 1999). 8,046 *T*ClpB particles were selected from micrographs with defocus values ranging from −1.5 μm to −2.4 μm using the BOXER application in EMAN (Ludtke et al., 1999). The contrast transfer function (CTF) correction was done with the program CTFIT (Ludtke et al., 1999) using structure factors that were generated from a preliminary model of the *T*ClpB hexamer (data not shown). The starting model for the reconstruction was generated using the reference-free classification method with no symmetry applied. This model was then refined over eight iterations using C_6 symmetry, an angular step size of 5°, and CTF correction to produce the final reconstruction consisting of 6040 particles. The resolution of the final reconstruction is 21.3 Å and was determined by dividing the data set in half, performing two independent reconstructions, and then assessing their Fourier shell correlation at a threshold of 0.5.

Fitting of *T*ClpB into the Cryo-EM Map

The atomic structure of an N-terminal domain truncated *T*ClpB-AMPPNP was manually fitted into the cryo-EM map as two rigid bodies, consisting of the D1 and D2 domain, respectively, using the program O (Jones et al., 1991). A model for the *T*ClpB hexamer was generated from the initial fit to confirm that there are no steric clashes among the protein main chain atoms. To refine the orientation of the manual fits, a molecular mask was calculated for each rigid body fragment using the program MAMA (Kleywegt and Jones, 1999). The masks were refined locally using the program IMP (Jones, 1992) to maximize the correlation between the search object (mask) and the density map of the *T*ClpB reconstruction. The two fragments were then connected by moving residues 536–544 as a rigid body. The resulting Cα-Cα distance between residues 535 and 536, and residues 544 and 545 were 3.6 Å and 3.8 Å, respectively. This places the D1 domain directly above the D2 domain of the same subunit. Connecting the D1 and D2 domains in a staggered conformation was not possible. The hexamer was generated by applying a 6-fold rotational symmetry matrix, which resulted in a unique fit that did not show any steric clashes among the protein main chain atoms. The final crosscorrelation coefficient between the fitted *T*ClpB hexamer and the cryo-EM map is 0.83 as calculated using FOLDHUNTER (Jiang et al., 2001).

Biochemical Assays

Mutants were generated and purified essentially as described (Watanabe et al., 2002). Prior to the first chromatography step, the bacterial cell extract was pasteurized at 80°C for 40 min. The chaperone activity was measured using a *T*ClpB-dependent reactivation assay at 55°C, after a 90 min incubation of *T*ClpB (0.05 μM; hexamer) with *B. stearothermophilus* G6PDH (0.2 μM; monomer), which had been heat-denatured by an 8 min incubation at 72°C in the presence of 0.2 μM *T*DnaK-DnaJ complex (trimer), 0.1 μM *T*GrpE (dimer), and 3 mM ATP. The assay was carried out in 50 mM MOPS-NaOH pH 7.5, 150 mM KCl, 5 mM $MgCl_2$, and in either the absence or the presence of 5 mM DTT. The chaperone activities of the leucine to alanine mutations were only measured in the presence of DTT. The oligomeric state of the *T*ClpB mutants was determined by analytical size-exclusion chromatography as described (Watanabe et al., 2002). The ATPase activities of *T*ClpB were measured at 50°C using an ATP-regenerating system (Stiggall et al., 1979) supplemented with 5 mM DTT and/or 0.1 mg/ml α-casein as appropriate.

Acknowledgments

We thank S.J. Ludtke and G. Decker for help with the cryo-EM; T. Kawashima for help with data collection; and the staff of APS-SBC 19ID (A. Joachimiak), NSLS X25 (M. Becker, L. Berman, and R. Sweet), and MacCHESS (D. Thiel) for access to and help with their respective synchrotron radiation light sources. S.L. acknowledges initial support by HHMI. W.C. is supported by a grant from NCRR P41RR02250. F.T.F.T. is supported by the American Heart Association (0130124N), the Welch Foundation (Q-1530), and the Gillson Longenbaugh Foundation.

Received: July 10, 2003
Revised: September 2, 2003
Accepted: September 29, 2003
Published: October 16, 2003

References

Barnett, M.E., Zolkiewska, A., and Zolkiewski, M. (2000). Structure and activity of ClpB from *Escherichia coli*. Role of the amino- and carboxyl-terminal domains. J. Biol. Chem. *275*, 37565–37571.

Beinker, P., Schlee, S., Groemping, Y., Seidel, R., and Reinstein, J. (2002). The N-terminus of ClpB from *Thermus thermophilus* is not essential for the chaperone activity. J. Biol. Chem. *277*, 47160–47166.

Beuron, F., Maurizi, M.R., Belnap, D.M., Kocsis, E., Booy, F.P., Kessel, M., and Steven, A.C. (1998). At sixes and sevens: characterization of the symmetry mismatch of the ClpAP chaperone-assisted protease. J. Struct. Biol. *123*, 248–259.

Brünger, A.T., Adams, P.D., Clore, G.M., DeLano, W.I., Gros, P., Grosse-Kunstleve, R.W., Jiang, J.-S., Kuszewski, J., Nilges, M., Pannu, N.S., et al. (1998). Crystallography & NMR system: a new software suite for macromolecular structure determination. Acta Crystallogr. D. *54*, 905–921.

Cashikar, A.G., Schirmer, E.C., Hattendorf, D.A., Glover, J.R., Ramakrishnan, M.S., Ware, D.M., and Lindquist, S.L. (2002). Defining a pathway of communication from the C-terminal peptide binding domain to the N-terminal ATPase domain in a AAA protein. Mol. Cell *9*, 751–760.

CCP4 (Collaborative Computational Project 4) (1994). The CCP4 suite: programs for protein crystallography. Acta Crystallogr. D. *50*, 760–763.

Clarke, A.K., and Eriksson, M.J. (2000). The truncated form of the bacterial heat shock protein ClpB/HSP100 contributes to development of thermotolerance in the cyanobacterium Synechococcus sp. strain PCC 7942. J. Bacteriol. *182*, 7092–7096.

de la Fortelle, E., and Bricogne, G. (1997). Maximum-likelihood heavy-atom parameter refinement in the MIR and MAD methods. Methods Enzymol. *276*, 472–494.

Diamant, S., Ben-Zvi, A.P., Bukau, B., and Goloubinoff, P. (2000). Size-dependent disaggregation of stable protein aggregates by the DnaK chaperone machinery. J. Biol. Chem. *275*, 21107–21113.

Dougan, D.A., Reid, B.G., Horwich, A.L., and Bukau, B. (2002). ClpS, a substrate modulator of the ClpAP machine. Mol. Cell *9*, 673–683.

Ellenberger, T.E., Brandl, C.J., Struhl, K., and Harrison, S.C. (1992). The GCN4 basic region leucine zipper binds DNA as a dimer of uninterrupted alpha helices: crystal structure of the protein-DNA complex. Cell *71*, 1223–1237.

Esnouf, R.M. (1997). An extensively modified version of MolScript that includes greatly enhanced coloring capabilities. J. Mol. Graph. Model. *15*, 132–134.

Gilson, M.K., Sharp, K., and Honig, B. (1987). Calculating the electrostatic potential of molecules in solution: method and error assessment. J. Comb. Chem. *9*, 327–335.

Glover, J.R., and Lindquist, S. (1998). Hsp104, Hsp70, and Hsp40: a novel chaperone system that rescues previously aggregated proteins. Cell *94*, 73–82.

Goloubinoff, P., Mogk, A., Zvi, A.P., Tomoyasu, T., and Bukau, B. (1999). Sequential mechanism of solubilization and refolding of stable protein aggregates by a bichaperone network. Proc. Natl. Acad. Sci. USA *96*, 13732–13737.

Guo, F., Maurizi, M.R., Esser, L., and Xia, D. (2002). Crystal structure of ClpA, an HSP100 chaperone and regulator of ClpAP protease. J. Biol. Chem. *277*, 46743–46752.

Ishikawa, T., Beuron, F., Kessel, M., Wickner, S., Maurizi, M.R., and Steven, A.C. (2001). Translocation pathway of protein substrates in ClpAP protease. Proc. Natl. Acad. Sci. USA *98*, 4328–4333.

Jiang, W., Baker, M.L., Ludtke, S.J., and Chiu, W. (2001). Bridging the information gap: computational tools for intermediate resolution structure interpretation. J. Mol. Biol. *308*, 1033–1044.

Jones, T.A. (1992). A, yaap, asap, @#*? A set of averaging programs. In Molecular Replacement, E.J. Dodson, S. Glover, and W. Wolf, eds. (Warrington, UK, Daresbury Laboratory), pp. 91–105.

Jones, T.A., Zou, J.Y., Cowan, S.W., and Kjeldgaard, M. (1991). Improved methods for binding protein models in electron density maps and the location of errors in these models. Acta Crystallogr. A *47*, 110–119.

Kim, K.I., Burton, R.E., Burton, B.M., Sauer, R.T., and Baker, T.A. (2000a). Dynamics of substrate denaturation and translocation by the ClpXP degradation machine. Mol. Cell *5*, 639–648.

Kim, K.I., Cheong, G.-W., Park, S.-C., Ha, J.-S., Woo, K.M., Choi, S.J., and Chung, C.H. (2000b). Heptameric ring structure of the heat-shock protein ClpB, a protein-activated ATPase in *Escherichia coli*. J. Mol. Biol. *303*, 655–666.

Kleywegt, G.J., and Jones, T.A. (1999). Software for handling macromolecular envelopes. Acta Crystallogr. D *55*, 941–944.

Kraulis, P. (1991). MOLSCRIPT: a program to produce both detailed and schematic plots of protein structures. J. Appl. Crystallogr. *24*, 946–950.

Li, J., and Sha, B. (2002). Crystal structure of *E. coli* Hsp100 ClpB nucleotide-binding domain 1 (NBD1) and mechanistic studies on ClpB ATPase activity. J. Mol. Biol. *318*, 1127–1137.

Li, J., and Sha, B. (2003). Crystal structure of the *E. coli* Hsp100 ClpB N-terminal domain. Structure *11*, 323–328.

Ludtke, S.J., Baldwin, P.R., and Chiu, W. (1999). EMAN: semiautomated software for high-resolution single-particle reconstructions. J. Struct. Biol. *128*, 82–97.

Merritt, E.A., and Bacon, D.J. (1997). Raster3D: photorealistic molecular graphics. Methods Enzymol. *277*, 505–524.

Mogk, A., Tomoyasu, T., Goloubinoff, P., Rüdiger, S., Röder, D., Langen, H., and Bukau, B. (1999). Identification of thermolabile *Escherichia coli* proteins: prevention and reversion of aggregation by DnaK and ClpB. EMBO J. *18*, 6934–6949.

Mogk, A., Schlieker, C., Strub, C., Rist, W., Weibezahn, J., and Bukau, B. (2003). Roles of individual domains and conserved motifs of the AAA+ chaperone ClpB in oligomerization, ATP hydrolysis, and chaperone activity. J. Biol. Chem. *278*, 17615–17624.

Motohashi, K., Watanabe, Y., Yohda, M., and Yoshida, M. (1999). Heat-inactivated proteins are rescued by the DnaK.J-GrpE set and ClpB chaperones. Proc. Natl. Acad. Sci. USA *96*, 7184–7189.

Neuwald, A.F., Aravind, L., Spouge, J.L., and Koonin, E.V. (1999). AAA+: a class of chaperone-like ATPases associated with the assembly, operation, and disassembly of protein complexes. Genome Res. *9*, 27–43.

Ogura, T., and Wilkinson, A.J. (2001). AAA+ superfamily ATPases: common structure-diverse function. Genes Cells *6*, 575–597.

Ortega, J., Singh, S.K., Ishikawa, T., Maurizi, M.R., and Steven, A.C. (2000). Visualization of substrate binding and translocation by the ATP-dependent protease, ClpXP. Mol. Cell *6*, 1515–1521.

O'Shea, E.K., Klemm, J.D., Kim, P.S., and Alber, T. (1991). X-ray structure of the GCN4 leucine zipper, a two-stranded, parallel coiled coil. Science *254*, 539–544.

Otwinowski, Z., and Minor, W. (1997). Processing of X-ray diffraction data collected in oscillation mode. Methods Enzymol. *276*, 307–326.

Park, S.-K., Kim, K.I., Woo, K.M., Seol, J.H., Tanaka, K., Ichihara, A., Ha, D.B., and Chung, C.H. (1993). Site-directed mutagenesis of the dual translational initiation sites of the clpB gene of *Escherichia coli* and characterization of its gene products. J. Biol. Chem. *268*, 20170–20174.

Parsell, D.A., Kowal, A.S., and Lindquist, S. (1994a). *Saccharomyces cerevisiae* Hsp104 protein. J. Biol. Chem. *269*, 4480–4487.

Parsell, D.A., Kowal, A.S., Singer, M.A., and Lindquist, S. (1994b). Protein disaggregation mediated by heat-shock protein Hsp104. Nature *372*, 475–478.

Scheffzek, K., Ahmadian, M.R., Kabsch, W., Wiesmuller, L., Lautwein, A., Schmitz, F., and Wittinghofer, A. (1997). The Ras-RasGAP complex: structural basis for GTPase activation and its loss in oncogenic Ras mutants. Science *277*, 333–338.

Schirmer, E.C., Glover, J.R., Singer, M.A., and Lindquist, S. (1996). Hsp100/Clp proteins: a common mechanism explains diverse functions. Trends Biochem. Sci. *21*, 289–296.

Schlee, S., Groemping, Y., Herde, P., Seidel, R., and Reinstein, J. (2001). The chaperone function of ClpB from *Thermus thermophilus* depends on allosteric interactions of its two ATP-binding sites. J. Mol. Biol. *306*, 889–899.

Smith, C.K., Baker, T.A., and Sauer, R.T. (1999). Lon and Clp family proteases and chaperones share homologous substrate-recognition domains. Proc. Natl. Acad. Sci. USA *96*, 6678–6682.

Stiggall, D.L., Galante, Y.M., and Hatefi, Y. (1979). Preparation and properties of complex V. Methods Enzymol. *55*, 308–315.

Tek, V., and Zolkiewski, M. (2002). Stability and interactions of the amino-terminal domain of ClpB from *Escherichia coli*. Protein Sci. *11*, 1192–1198.

Vale, R.D. (2000). AAA proteins: lords of the ring. J. Cell Biol. *150*, F13–F19.

Walker, J.E., Saraste, M., Runswick, M.J., and Gay, N.J. (1982). Distantly related sequences in the alpha- and beta-subunits of ATP synthase, myosin, kinases and other ATP-requiring enzymes and a common nucleotide binding fold. EMBO J. *1*, 945–951.

Wang, J., Song, J.J., Seong, I.S., Franklin, M.C., Kamtekar, S., Eom, S.H., and Chung, C.H. (2001). Nucleotide-dependent conformational changes in a protease-associated ATPase HslU. Structure *9*, 1107–1116.

Watanabe, Y.-H., Motohashi, K., and Yoshida, M. (2002). Roles of the two ATP binding sites of ClpB from *Thermus thermophilus*. J. Biol. Chem. *277*, 5804–5809.

Weber-Ban, E.U., Reid, B.G., Miranker, A.D., and Horwich, A.L. (1999). Global unfolding of a substrate protein by the Hsp100 chaperone ClpA. Nature *401*, 90–93.

Wickner, S., Maurizi, M.R., and Gottesman, S. (1999). Posttranslational quality control: folding, refolding, and degrading proteins. Science *286*, 1888–1893.

Zolkiewski, M. (1999). ClpB cooperates with DnaK, DnaJ, and GrpE in suppressing protein aggregation. J. Biol. Chem. *274*, 28083–28086.

Zolkiewski, M., Kessel, M., Ginsburg, A., and Maurizi, M.R. (1999). Nucleotide-dependent oligomerization of ClpB from *Escherichia coli*. Protein Sci. *8*, 1899–1903.

Accession Numbers

Coordinates have been deposited with the Protein Data Bank (accession number 1QVR).